Defect-Mediated Morphologies in Growing Cell Colonies

Amin Doostmohammadi, Sumesh P. Thampi, and Julia M. Yeomans*
The Rudolf Peierls Centre for Theoretical Physics, 1 Keble Road, Oxford OX1 3NP, United Kingdom
(Received 13 December 2015; published 20 July 2016)

Morphological trends in growing colonies of living cells are at the core of physiological and evolutionary processes. Using active gel equations, which include cell division, we show that shape changes during the growth can be regulated by the dynamics of topological defects in the orientation of cells. The friction between the dividing cells and underlying substrate drives anisotropic colony shapes toward more isotropic morphologies, by mediating the number density and velocity of topological defects. We show that the defects interact with the interface at a specific interaction range, set by the vorticity length scale of flows within the colony, and that the cells predominantly reorient parallel to the interface due to division-induced active stresses.

DOI: 10.1103/PhysRevLett.117.048102

Growth dynamics is of considerable importance in biological processes, from biofilm formation to morphogenesis and tumor invasion [1–3]. A prominent feature in these systems is the emergence of coordinated motion of constituent cells, which may be affected by several mechanisms such as biological signals [4], chemical cues [5,6], and mechanical stimuli [7]. Recent experimental studies of bacterial colonies and cellular assemblies show growing evidence of the role of mechanical factors in regulating growth and collective migration [8–16]. In particular, the emergence of collective motion of cells is often connected to the generation of active stresses by molecular motors and actin polymerization dynamics and by cell division [17–19]. Within this context cellular assemblies and bacterial colonies can be modeled as active gels, and the equations of active nematic liquid crystals have been shown to reproduce several experimental observations such as the collective migration of cells [20–22] and the flow fields of dividing cells [19].

The relevance of nematic models is highlighted in Fig. 1, which shows a snapshot of a dividing *E. coli* colony. The orientation field of the rod-shaped *E. coli* shows clear local nematic order, corresponding to alignment of the bacteria. *Topological defects* can also be identified. Such defects cannot be removed by a local realignment of the orientation, and at a defect core the ordering is destroyed. The strength of a defect is measured as the change in the nematic orientation following a closed curve around the defect core [23]. Therefore $\pm 1/2$ defects, identified in Fig. 1, correspond to $\pm\pi$ rotations of the bacterial orientation around the defect. Note also the preferential alignment of the cells tangential to the surface. The emergence of half integer defects shows that although a single eukaryotic cell or single *E. coli* bacterium is polar, monolayers consisting of several cells or a suspension of bacteria are nematics. The nematic order and topological defects have been reported for bacterial colonies (Fig. 1), cultures of fibroblast [24,25], in living amoeboid cells [26], and more recently in stem cells [27] and Madin-Darby canine kidney (MDCK) cells [28]. However, to the best of our knowledge, the role of topological defects in growth dynamics and their connections to the morphological responses of cell cultures have not yet been explored.

Here, we show how the dynamics of topological defects contribute to shape changes in growing colonies of dividing cells. Building on the active gel description of cellular layers [19,22], we show that the progression of the interface and its morphology are correlated with the generation of defects and their dynamics. In addition, we relate friction between cells and the underlying substrate to conformational changes based on the increase in defects density and reduction of their velocities with increasing friction.

To represent the dynamics of a growing colony, we use a continuum description of cells as an active gel growing in an isotropic liquid [19,29–32]. The fields that describe the system are the total density ρ, the concentration of cells φ

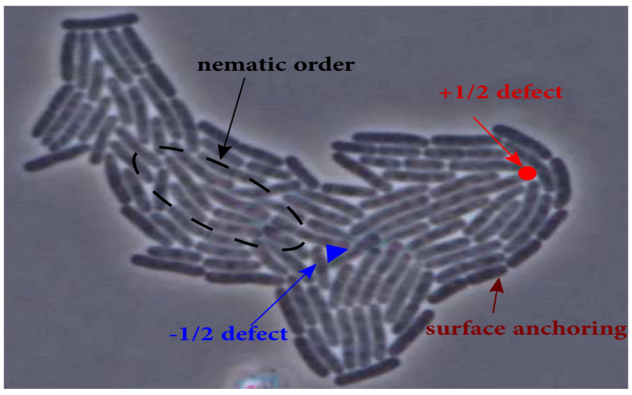

FIG. 1. A growing *E. coli* colony shows nematic ordering, $\pm 1/2$ topological defects, and tangential alignment to the interface (Picture courtesy of Lin Chao, to whom all rights are reserved).

which is close to 1 within the colony and close to 0 outside, the velocity $\boldsymbol{u}$, and the nematic order parameter $\mathbf{Q} = 2q(\mathbf{nn} - \mathbf{I}/2)$, where $\mathbf{n}$ is the director and q the magnitude of the nematic order. Note that φ is a binary fluid order parameter used to distinguish the two fluids, while ρ is the total density of nematic and isotropic liquids. In the continuum formulation the velocity of individual cells is not the quantity of interest. Here, the velocity field $\boldsymbol{u}$ describes the coarse-grained velocity of the cell and fluid medium (averaged over a given volume).

The nematic tensor obeys

$$(\partial_t + \boldsymbol{u}\cdot\boldsymbol{\nabla})\boldsymbol{Q} - \boldsymbol{S} = \Gamma_Q \boldsymbol{H}, \tag{1}$$

where $\boldsymbol{S} = \lambda\boldsymbol{E} - (\boldsymbol{\omega}\cdot\boldsymbol{Q} - \boldsymbol{Q}\cdot\boldsymbol{\omega})$ is a generalized advection term [33], characterizing the response of the nematic tensor to velocity gradients. Here, $\boldsymbol{E} = (\boldsymbol{\nabla u} + \boldsymbol{\nabla u}^T)/2$ is the strain rate tensor and $\boldsymbol{\omega} = (\boldsymbol{\nabla u}^T - \boldsymbol{\nabla u})/2$ is the vorticity tensor. The alignment parameter λ is related to the shape of active particles with $\lambda > 0$ for rodlike particles, $\lambda < 0$ for disklike particles, and $\lambda = 0$ for spherical particles. We are strictly in two dimensions, and there is no source or sink of mass due to flow from the third direction. Thus, the velocity field is divergence free and $\boldsymbol{E}$ is traceless. We note that in experiments of growing cell colonies there are often flows of nutrients from the third dimension to avoid starvation of cells. Such flows from the third dimension could impact the mass conservation in a two-dimensional colony. In Eq. (1), Γ_Q is a rotational diffusivity and the molecular field $\boldsymbol{H} = -(\partial\mathcal{F}_{\mathrm{LC}}/\partial\boldsymbol{Q}) + \nabla\cdot(\partial\mathcal{F}_{\mathrm{LC}}/\partial\nabla\boldsymbol{Q})$ models the relaxation of the orientational order to minimize a free energy with density $\mathcal{F}_{\mathrm{LC}} = \frac{1}{2}A(q_n^2\varphi - \frac{1}{2}\mathrm{tr}(\boldsymbol{Q}^2))^2 + \frac{1}{2}K(\boldsymbol{\nabla Q})^2$, where K and A are material constants and the coupling ensures that nematic order with $q = q_n$ is favored for $\varphi \approx 1$ and vanishes in the isotropic phase ($\varphi \approx 0$). Cell division, modeled as a growth term in the evolution equation for φ thus refers to conversion of isotropic fluid to a fluid of liquid crystalline order. The assumption of an incompressible tissue and modeling the coarse-grained velocity of cells has been extensively employed in studies of cell division and in reproducing experimental observations [18,20,21,34,35].

The concentration of cells follows:

$$\partial_t\varphi + \boldsymbol{\nabla}\cdot(\boldsymbol{u}\varphi) = \Gamma_\varphi\boldsymbol{\nabla}^2\mu + \alpha\varphi, \tag{2}$$

where Γ_φ is the mobility, α is the division rate, $\mu = (\partial\mathcal{F}/\partial\varphi) - \boldsymbol{\nabla}\cdot(\partial\mathcal{F}/\partial\boldsymbol{\nabla}\varphi)$ is the chemical potential, and the free energy density $\mathcal{F} = \mathcal{F}_{\mathrm{LC}} + \mathcal{F}_{\mathrm{GL}}$ includes additional contributions from Ginzburg-Landau free energy density $\mathcal{F}_{\mathrm{GL}} = (A_\varphi/2)\varphi^2(1-\varphi)^2 + (K_\varphi/2)(\boldsymbol{\nabla}\varphi)^2$ to allow for phase ordering and surface tension between isotropic and nematic fluids [36]. The velocity $\mathbf{u}$ evolves according to

$$\rho(\partial_t + \boldsymbol{u}\cdot\boldsymbol{\nabla})\boldsymbol{u} = \boldsymbol{\nabla}\cdot\Pi - f_0\varphi\boldsymbol{u}, \tag{3}$$

where Π denotes the stress tensor with f_0 the friction coefficient between the cells and the underlying substrate. The stress contributions comprise the viscous stress $\Pi^{\mathrm{viscous}} = 2\eta\boldsymbol{E}$, where η is the viscosity, the elastic stresses $\Pi^{\mathrm{elastic}} = -P\boldsymbol{I} - \lambda\boldsymbol{H} + \boldsymbol{Q}\cdot\boldsymbol{H} - \boldsymbol{H}\cdot\boldsymbol{Q} - \boldsymbol{\nabla Q}:\partial\mathcal{F}/\partial\boldsymbol{\nabla Q}$, where P is the bulk pressure, and capillary stresses $\Pi^{\mathrm{cap}} = (\mathcal{F} - \mu\varphi)\boldsymbol{I} - \boldsymbol{\nabla}\varphi(\partial\mathcal{F}/\partial\boldsymbol{\nabla}\varphi)$.

A local increase in the concentration of cells, driven by the $\alpha\varphi$ term in Eq. (2), generates dipolelike flow fields and a growth pressure through the isotropic part of the capillary stress. These reproduce the experimentally measured flow fields of dividing MDCK cells and can be regarded as a source of active stress generation in cell monolayers [19]. In the simulations cell division events are introduced randomly across the domain as a local increase of $\alpha\varphi$ over a short time of t_0 time steps, in circles with radius of r_0 grid points.

Previous theoretical studies have examined the instability of interfaces subject to cell proliferation, neglecting orientational order of cells [34,37]. In the presence of orientational order, the deformation of the interface at early times is driven by bending instability of the director and nonlinear properties of the bulk [32] and cannot be explored by a simplified linear set of equations. Therefore, here we numerically solve Eqs. (1)–(3) using a hybrid lattice Boltzmann method [19,23,33,36,38–45].

An initially circular assembly of cells, with initial random orientations, grows in space as the cells begin to divide. At low friction the colony's shape is characterized by a number of fingerlike protrusions reaching into the isotropic liquid, while at higher friction the fingering is greatly reduced and the shape of the colony remains close to circular (Fig. 2).

A quantitative measure of the shape change can be obtained by calculating the isoperimetric quotient of the growing colony $\mathrm{IQ} = 4\pi\mathcal{A}/\mathcal{P}^2$, where $\mathcal{A}$ is the surface area

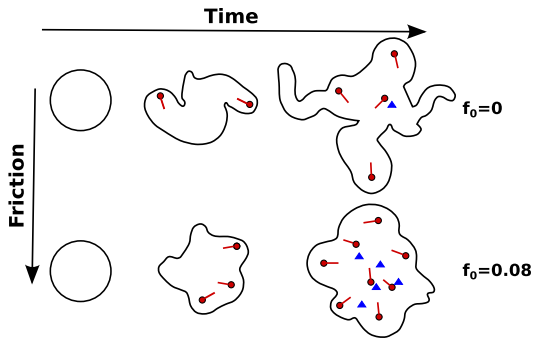

FIG. 2. The spatiotemporal evolution of a growing colony is affected by the dynamics of topological defects and by friction with the substrate. We show the interface of the colony (defined as contour line of $\varphi = 0.5$) and $+1/2$, $-1/2$ defects marked by red circles and blue triangles, respectively. The lines at the end of $+1/2$ defects represent the cometlike tail of defects characterizing their direction of motion (from tail to head).

and $\mathcal{P}$ is the perimeter of the cell assembly. For a perfect circular geometry IQ = 1, and it decreases as the shape deviates from a circle. At zero friction, the IQ drops rapidly as the initial circular geometry is perturbed by defect-induced protrusions [Fig. 3(a), red data] before flattening to an asymptotic value for longer times. The higher IQ measured for larger friction indicates the tendency towards forming a more circular morphology [Fig. 3(a), orange line].

The positions of $\pm 1/2$ topological defects are also shown in Fig. 2. The defects can be identified by calculating the diffusive charge density [32], $s=(1/2\pi)\times\{[(\partial Q_{xx}/\partial x)(\partial Q_{xy}/\partial y)]-[(\partial Q_{xx}/\partial y)(\partial Q_{xy}/\partial x)]\}$, which gives $s = \pm 1/2$ at the position of defect cores. The number density of defects increases with increasing friction until it saturates in the highly damped region, where the formation of extra defects becomes energetically costly [46,47] [Fig. 3(b), red data]. The number density of defects is inversely proportional to the square root of the distance between them, which is controlled by the characteristic length scale of the vorticity $N_d^2 \propto 1/l_\Omega$ [42]. Before reaching the highly damped region the vorticity length scale is expected to be proportional to the screening length $l_{sc} = \sqrt{\eta/\rho f_0}$, which is set by the competition between viscosity and friction [47]. Therefore $N_d \propto l_{sc}^{-1/2}$ [Fig. 3(c)]. Moreover the average defect velocity V_d decreases with increasing friction [Fig. 3(b), green data].

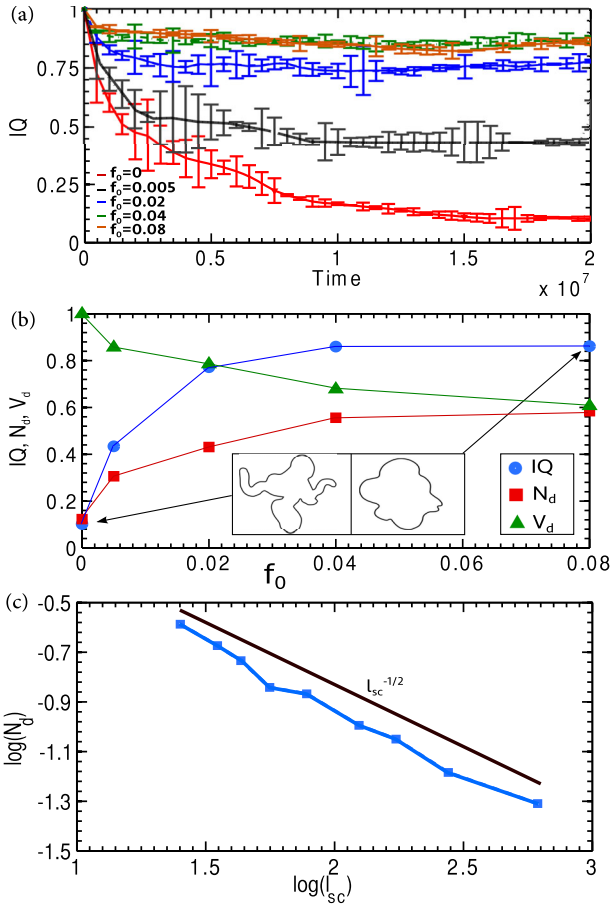

FIG. 3. Friction controls shape changes in a growing colony by affecting the dynamics of defects. (a) The conformational changes over time (characterized by IQ) as a function of friction. (b) Dependence on friction of IQ, the number density of defects N_d, and the average defect velocity V_d at long times. (c) Variation of the defect density as a function of the screening length $l_{sc} = \sqrt{\eta/\rho f_0}$ on a log-log plot for $f_0 \leq 0.04$, before entering the highly damped region.

Figure 4(a) shows in more detail how defects are created and annihilated. Defects can either be created at the interface (defects 1 and 4) due to surface undulations, leaving a net negative charge on the interface, or appear as a pair in the bulk (defect pair 2–3) to release elastic energy associated with the orientation field. Once created, $+1/2$ defects move through the colony and either annihilate with the oppositely charged defects in the bulk (defect 4 annihilates with defect 3) or approach the interface (defects 1 and 2). As a defect moves towards the interface the progression of the border adapts to the motion of the approaching defect until it reaches the surface and annihilates with the negative charge density that is distributed along the interface. This suggests that the shape of the colony will be correlated to the motion of the defects and it is apparent from Figs. 1 and 2 that fingerlike protrusions are closely linked to the motion of cometlike +1/2 defects.

When the friction is small, defects moving towards the border and the consequent protrusions are few in number and energetic, and the shape of a growing assembly is highly anisotropic (Fig. 2, top row). However, with increasing friction, the defects density increases and the average defect velocity drops resulting in a more isotropic morphology (Fig. 2, bottom row).

To obtain a more quantitative characterization of the connection between the movement of defects and progression of the interface, we define the cross-correlation function between defect and interface velocities $C_{D-I}(r) = \langle \boldsymbol{v}_D(r,t)\cdot\boldsymbol{v}_I(r,t)\rangle/\langle \boldsymbol{v}_D(0,t)\cdot\boldsymbol{v}_I(0,t)\rangle$, where $\boldsymbol{v}_D = \Delta d_D/\Delta t$ denotes the defect velocity and $\boldsymbol{v}_I = \Delta d_I/\Delta t$ is the velocity of the point on the interface at a distance r from the defect in the direction of $\boldsymbol{v}_D$ [see Fig. 4(b), inset]. The measurement of C_{D-I} demonstrates that the defect and interface displacements are correlated over a given distance, which we term the *interaction range* [Fig. 4(b)]. This interaction range decreases as the friction is increased.

To determine the physical mechanism for the emergence of the interaction range and its dependence on the friction, we consider the flow field and director configuration around a defect approaching the interface [Fig. 4(c)]. As evident from the figure the motion of the defect sets up counter-rotating velocity vortices [45,48,49]. We conjecture that the interaction range is controlled by the vorticity length scale in the growing colony. To show that this is

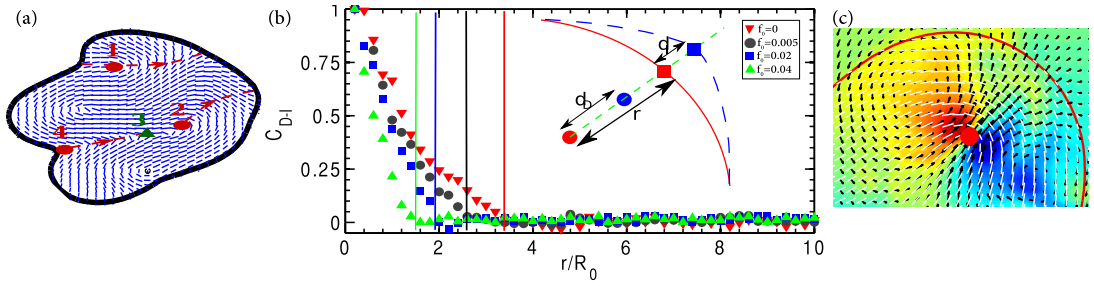

FIG. 4. The displacement of the interface is correlated with the motion of nearby defects. (a) The typical trajectories of topological defects created at the interface (1,4) or as a pair in the bulk (2–3). The director field is shown by blue solid lines and $+1/2$, $-1/2$ defects are illustrated by red circles and green triangles, respectively. (b) The defect-interface cross-correlation for different frictions versus distance normalized by the initial radius of the colony R_0 and (c) the flow field around a defect moving towards the interface. Vertical solid lines in (b) correspond to the characteristic vorticity length scale at different frictions. The inset in (b) shows a schematic of the displacements of a defect (circle) and the interface (line). The position of the nearest point at the interface along the direction of the defect velocity is marked by a square. Red and blue colors correspond to consecutive positions at times t and $t+1$, respectively. The color map in (c) illustrates the vorticity contours, superimposed by velocity vectors (black arrows) and cell orientations (white solid lines).

indeed the case we calculate the characteristic vorticity length scale from the vorticity-vorticity correlation function and compare it to the interaction range for different frictions [Fig. 4(b), solid lines]. The close agreement between the length scales of the vorticity and the defect-interface interaction range shows that the defect motion towards the interface affects the interface deformation through vortex generation around a defect. As the friction is increased the vorticity field is more effectively suppressed by hydrodynamic screening and therefore the characteristic vorticity length is reduced [47], leading to a shorter interaction range between defects and the interface [Fig. 4(b)].

An interesting feature observed during the simulated growth of the cell colony is that cells at the border tend to lie parallel to the interface. This is quantified by plotting the distribution of the anchoring angle relative to the interface of the outermost cells (Fig. 5). Similar behavior is evident in Fig. 1 and in the experiments reported in [31]. In a recent study of lyotropic active nematics Blow *et al.* [32] showed that the gradients in order and orientation of nematogens along an interface result in the generation of activity-induced anchoring forces which, for extensile active nematics, induce tangential orientations along the interface.

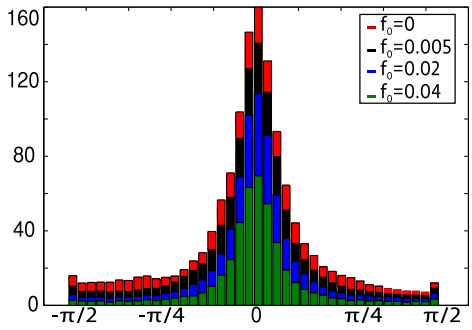

FIG. 5. Dividing cells align along the free surface: distribution of anchoring angle relative to the surface for different frictions.

Since the cell division generates extensile stresses [19], we expect the same mechanism to be responsible for the anchoring along the border of a growing colony.

It has been shown recently that by increasing the adhesion between the cells and substrate the spreading of cell aggregates is enhanced: groups of cells are formed in the shape of fingerlike structures leading to anisotropic shapes [50]. This was interpreted in terms of "leader" cells at the end of the fingers. By contrast previous theoretical predictions have associated the fingering to the curvature dependent motility of cells [51] or undulation instabilities due to cell proliferation in epithelial tissues [34,37], neglecting the orientational order of cells. Here, we offer an alternative, collective physical mechanism for morphological changes based on the dynamics of topological defects. To test these ideas the friction between cells and their underlying substrate could be used to vary defects density [46,47,52]. A potential approach would be to consider a fixed amount of fibronectine proteins, which control cell binding to the substrate, and explore the spreading dynamics on substrates with varying stiffness to introduce differing hydrodynamic screening [28]. Indeed theoretical predictions [53,54] and recent experiments do show the role of friction in pattern formation in active matter [52,55].

We have described a new physical mechanism for understanding morphological changes in growing colonies based on the dynamics of topological defects in cell orientations. Such defects have been recently observed experimentally [25,27,28] and our results suggest directions for further investigations of defect-mediated migration and morphologies in cellular colonies.

We acknowledge funding from the ERC Advanced Grant (MiCE 291234). We thank Matthew Blow, Benoit Ladoux, Romain Mueller, Wilson Poon, Thuan Beng Saw, Tyler Shendruk, and Ben Simons for helpful discussions.

*j.yeomans1@physics.ox.ac.uk

[1] L. Hall-Stoodley, J. W. Costerton, and P. Stoodley, Nat. Rev. Microbiol. **2**, 95 (2004).
[2] K. Ghosh and D. E. Ingber, Adv. Drug Delivery Rev. **59**, 1306 (2007).
[3] P. Lee and C. W. Wolgemuth, PLoS Comput. Biol. **7**, e1002007 (2011).
[4] P. Haas and D. Gilmour, Dev. Cell **10**, 673 (2006).
[5] J. M. Tse, C. Gang, J. A. Tyrrell, S. A. Wilcox-Adelman, Y. Boucher, K. J. Rakesh, and L. L. Munn, Proc. Natl. Acad. Sci. U.S.A. **109**, 911 (2012).
[6] A. Gelimson and R. Golestanian, Phys. Rev. Lett. **114**, 028101 (2015).
[7] X. Trepat and J. J. Fredberg, Trends Cell Biol. **21**, 638 (2011).
[8] M. A. A. Grant, B. Wacław, R. J. Allen, and P. Cicuta, J. R. Soc. Interface **11**, 20140400 (2014).
[9] D. P. Lloyd and R. J. Allen, J. R. Soc. Interface **12**, 20150608 (2015).
[10] G. Melaugh, J. Hutchison, K. N. Kragh, Y. Irie, A. Roberts, T. Bjarnsholt, S. P. Diggle, V. Gordon, and R. J. Allen, arXiv:1506.08168.
[11] X. Trepat, M. R. Wasserman, T. E. Angelini, E. Millet, D. A. Weitz, J. P. Butler, and J. J. Fredberg, Nat. Phys. **5**, 426 (2009).
[12] D. T. Tambe, C. C. Hardin, T. E. Angelini, K. Rajendran, C. Y. Park, X. Serra-Picamal, E. H. Zhou, M. H. Zaman, J. P. Butler, D. A. Weitz *et al.*, Nat. Mater. **10**, 469 (2011).
[13] S. R. K. Vedula, M. C. Leong, T. L. Lai, P. Hersen, A. J. Kabla, C. T. Lim, and B. Ladoux, Proc. Natl. Acad. Sci. U.S.A. **109**, 12974 (2012).
[14] K. Doxzen, S. R. K. Vedula, M. C. Leong, H. Hirata, N. S. Gov, A. J. Kabla, B. Ladoux, and C. T. Lim, Integr. Biol. **5**, 1026 (2013).
[15] D. Ott, P. M. Bendix, and L. B. Oddershede, ACS Nano **7**, 8333 (2013).
[16] H. Klingberg, L. B. Oddershede, S. Loft, and P. Møller, Nanoscale **7**, 11409 (2015).
[17] J. Ranft, M. Basan, J. Elgeti, J. F. Joanny, J. Prost, and F. Jülicher, Proc. Natl. Acad. Sci. U.S.A. **107**, 20863 (2010).
[18] N. S. Rossen, J. M. Tarp, J. Mathiesen, M. H. Jensen, and L. B. Oddershede, Nat. Commun. **5**, 5720 (2014).
[19] A. Doostmohammadi, S. P. Thampi, T. B. Saw, C. T. Lim, B. Ladoux, and J. M. Yeomans, Soft Matter **11**, 7328 (2015).
[20] T. Bittig, O. Wartlick, A. Kicheva, M. González-Gaitán, and F. Jülicher, New J. Phys. **10**, 063001 (2008).
[21] T. Bittig, O. Wartlick, M. González-Gaitán, and F. Jülicher, Eur. Phys. J. Spec. Top. **30**, 93 (2009).
[22] J. Prost, F. Jülicher, and J. F. Joanny, Nat. Phys. **11**, 111 (2015).
[23] P. G. de Gennes and J. Prost, *The Physics of Liquid Crystals* (Oxford University Press, Oxford, England, 1995).
[24] T. Elsdale and F. Wasoff, Dev. Biol. **180**, 121 (1976).
[25] G. Duclos, S. Garcia, H. Yevick, and P. Silberzan, Soft Matter **10**, 2346 (2014).
[26] H. Gruler, U. Dewald, and M. Eberhardt, Eur. Phys. J. Spec. Top. **11**, 187 (1999).
[27] K. Kawaguchi, R. Kageyama, and M. Sano, arXiv:1605.06470.
[28] B. Ladoux (personal communications).
[29] K. Kruse, J. F. Joanny, F. Jülicher, J. Prost, and K. Sekimoto, Eur. Phys. J. E **16**, 5 (2005).
[30] J. F. Joanny, F. Jülicher, K. Kruse, and J. Prost, New J. Phys. **9**, 422 (2007).
[31] D. Volfson, S. Cookson, J. Hasty, and L. S. Tsimring, Proc. Natl. Acad. Sci. U.S.A. **105**, 15346 (2008).
[32] M. L. Blow, S. P. Thampi, and J. M. Yeomans, Phys. Rev. Lett. **113**, 248303 (2014).
[33] A. N. Beris and B. J. Edwards, *Thermodynamics of Flowing Systems* (Oxford University Press, Oxford, England, 1994).
[34] M. Basan, J. F. Joanny, J. Prost, and T. Risler, Phys. Rev. Lett. **106**, 158101 (2011).
[35] M. Delarue, F. Montel, O. Caen, J. Elgeti, J. M. Siaugue, D. Vignjevic, J. Prost, J. F. Joanny, and G. Cappello, Phys. Rev. Lett. **110**, 138103 (2013).
[36] J. W. Cahn and J. E. Hilliard, J. Chem. Phys. **28**, 258 (1958).
[37] T. Risler, A. Peilloux, and J. Prost, Phys. Rev. Lett. **115**, 258104 (2015).
[38] See Supplemental Material at http://link.aps.org/supplemental/10.1103/PhysRevLett.117.048102, which includes Refs. [19, 23, 33, 36, 39–45], for the details of simulations and the choice of parameters.
[39] C. Denniston, D. Marenduzzo, E. Orlandini, and J. M. Yeomans, Phil. Trans. R. Soc. A **362**, 1745 (2004).
[40] D. Marenduzzo, E. Orlandini, M. E. Cates, and J. M. Yeomans, Phys. Rev. E **76**, 031921 (2007).
[41] S. M. Fielding, D. Marenduzzo, and M. E. Cates, Phys. Rev. E **83**, 041910 (2011).
[42] S. P. Thampi, R. Golestanian, and J. M. Yeomans, Phil. Trans. R. Soc. A **372**, 20130366 (2014).
[43] L. Giomi, L. Mahadevan, B. Chakraborty, and M. F. Hagan, Phys. Rev. Lett. **106**, 218101 (2011).
[44] T. Sanchez, D. T. N. Chen, S. J. DeCamp, M. Heymann, and Z. Dogic, Nature (London) **491**, 431 (2012).
[45] S. P. Thampi, R. Golestanian, and J. M. Yeomans, Phys. Rev. Lett. **111**, 118101 (2013).
[46] S. P. Thampi, R. Golestanian, and J. M. Yeomans, Phys. Rev. E **90**, 062307 (2014).
[47] A. Doostmohammadi, M. F. Adamer, S. P. Thampi, and J. M. Yeomans, Nat. Commun. **7**, 10557 (2016).
[48] G. Tóth, C. Denniston, and J. M. Yeomans, Phys. Rev. Lett. **88**, 105504 (2002).
[49] L. Giomi, M. J. Bowick, X. Ma, and M. C. Marchetti, Phys. Rev. Lett. **110**, 228101 (2013).
[50] A. Ravasio, A. P. Le, T. B. Saw, V. Tarle, H. T. Ong, C. Bertocchi, R.-M. Mège, C. T. Lim, N. S. Gov, and B. Ladoux, Integr. Biol. **7**, 1228 (2015).
[51] L. Petitjean, M. Reffay, E. Grasland-Mongrain, M. Poujade, B. Ladoux, A. Buguin, and P. Silberzan, Biophys. J. **98**, 1790 (2010).
[52] P. Guillamat, J. Ignés-Mullol, and F. Sagués, Proc. Natl. Acad. Sci. U.S.A. **113**, 5498 (2016).
[53] M. Mayer, M. Depken, J. S. Bois, F. Jülicher, and S. W. Grill, Nature (London) **467**, 617 (2010).
[54] J. S. Bois, F. Jülicher, and S. W. Grill, Phys. Rev. Lett. **106**, 028103 (2011).
[55] E. Hannezo, B. Dong, P. Recho, J. F. Joanny, and S. Hayashi, Proc. Natl. Acad. Sci. U.S.A. **112**, 8620 (2015).